Generating small-scale structures from large-scale ones via optical near-field interactions

M. Naruse[1, 2*], T. Yatsui[3], H. Hori[4], K. Kitamura[2], and M. Ohtsu[2]

[1]*National Institute of Information and Communications Technology, 4-2-1 Nukui-kita, Koganei, Tokyo 184-8795, Japan*
[2]*The University of Tokyo, 2-11-16 Yayoi, Bunkyo-ku, Tokyo 113-8656, Japan*
[3]*Japan Science and Technology Agency, 2-11-16 Yayoi, Bunkyo-ku, Tokyo 113-8656, Japan*
[4]*University of Yamanashi, 4-3-11 Takeda, Kofu, Yamanashi 400-8511, Japan*
**Corresponding author: naruse@nict.go.jp*

Abstract: Optical near-fields, which appear in the vicinity of structures when irradiated with light, exhibit a hierarchical nature, meaning that the degree of localization of optical near-fields at a given point is related to the scale of the structure involved in this process. Therefore, if we could make optically induced fabrication processes selectively localized in the near-field region, we could generate a smaller-scale structure even from a larger-scale one via optical near-field interactions. We demonstrate the theoretical basis of this with an angular spectrum analysis of optical near-fields. We also experimentally demonstrate such principles by using ZnO nanoneedles fabricated through metal-organic vapor phase epitaxy (MOVPE) followed by a photo-induced MOVPE procedure where smaller-scale generated structures were clearly observed with the help of light irradiation. We also observed that the generated fine structures followed a power-law distribution, indicating that fractal structures emerged via optical near-field interactions.

OCIS codes: (999.9999) Near-field optics; (220.4000) Microstructure fabrication; (260.2110) Electromagnetic optics; (140.3450) Laser-induced chemistry; (999.9999) Nanophotonics

References and links

1. M. Ohtsu, K. Kobayashi, T. Kawazoe, S. Sangu, and T. Yatsui, "Nanophotonics: design, fabrication, and operation of nanometric devices using optical near fields," IEEE J. Sel. Top. Quantum Electron. **8**, 839-862 (2002).
2. For example, T. Yatsui, M. Kourogi, K. Tsutsui, J. Takahashi, and M. Ohtsu, "High-density-speed optical near-field recording-reading with a pyramidal silicon probe on a contact slider," Opt. Lett. **25**, 1279-1281 (2000).
3. S.-J. Chen, F. C. Chien, G. Y. Lin, and K. C. Lee, "Enhancement of the resolution of surface plasmon resonance biosensors by control of the size and distribution of nanoparticles," Opt. Lett. **29**, 1390-1392 (2004).
4. T. Kawazoe, K. Kobayashi, S. Sangu, and M. Ohtsu, "Demonstration of a nanophotonic switching operation by optical near-field energy transfer," Appl. Phys. Lett. **82**, 2957-2959 (2003).
5. M. Naruse, T. Miyazaki, T. Kawazoe, K. Kobayashi, S. Sangu, F. Kubota, and M. Ohtsu, "Nanophotonic Computing Based on Optical Near-Field Interactions between Quantum Dots," IEICE Trans. Electron. **E88-C**, 1817-1823 (2005).
6. K. Matsuda, T. Saiki, S. Nomura, M. Mihara, Y. Aoyagi, S. Nair, and T. Takagahara, Phys. Rev. Lett. **91**, 177401 1-4 (2003).
7. T. Yatsui, G.-C. Yi, and M. Ohtsu, "Integration and evaluation of nanophotonic device," in *Progress in Nano-Electro-Optics V*, M. Ohtsu ed. (Springer, Berlin, 2006), 63-107.
8. T. Yatsui, S. Takubo, J. Lim, W. Nomura, M. Kourogi, and M. Ohtsu, "Regulating the size and position of deposited Zn nanoparticles by optical near-field desorption using size-dependent resonance," Appl. Phys. Lett. **83**, 1716-1718 (2003).
9. H. Yonemitsu, T. Kawazoe, K. Kobayashi, and M. Ohtsu, "Nonadiabatic photochemical reaction and application to photolithography," J. Luminescence **122-123**, 230-233 (2007).
10. B. Skoric, S. Maubach, T. Kevenaar, and P. Tuyls, "Information-theoretic analysis of capacitive physical unclonable functions," J. Appl. Phys. **100**, 024902 1-11 (2006).

#85246 - $15.00 USD Received 13 Jul 2007; revised 29 Aug 2007; accepted 29 Aug 2007; published 31 Aug 2007

11. T. Yatsui, W. Nomura, and M. Ohtsu, "Self-assembly of size- and position-controlled ultralong nanodot chains using near-field optical desorption," Nano. Lett. **5**, 2548- 2551 (2005).
12. P. Mühlschlegel, H.-J. Eisler, O. J. F. Martin, B. Hecht, and D. W. Pohl, "Resonant optical antennas," Science **308**, 1607-1609 (2005).
13. T. Matsumoto, T. Shimano, H. Saga, H. Sukeda, and M. Kiguchi, "Highly efficient probe with a wedge-shaped metallic plate for high density near-field optical recording," J. Appl. Phys. **95**, 3901-3906 (2004).
14. T. Yatsui, M. Kourogi, and M. Ohtsu, "Plasmon waveguide for optical far/near-field conversion," Appl. Phys. Lett. **79**, 4583-4585 (2001).
15. S. A. Maier, M. L. Brongersma, P. G. Kik, and H. A. Atwater, "Observation of near-field coupling in metal nanoparticle chains using far-field polarization spectroscopy," Phys. Rev. B **65**, 193408 1-4 (2002).
16. E. Wolf and M. Nieto-Vesperinas, "Analyticity of the angular spectrum amplitude of scattered fields and some of its consequences," J. Opt. Soc. Am. A. **2**, 886-890 (1985).
17. T. Inoue and H. Hori, "Quantum theory of radiation in optical near field based on quantization of evanescent electromagnetic waves using detector mode," in *Progress in Nano-Electro-Optics IV*, M. Ohtsu ed. (Springer Verlag, 2005), 127-199.
18. M. Naruse, T. Inoue, and H. Hori, "Analysis and synthesis of hierarchy in optical near-field interactions at the nanoscale based on angular spectrum," Jpn. J. Appl. Phys. in press.
19. W. I. Park, G.-C Yi, M. Kim, and S. J. Pennycook, "ZnO nanoneedles grown vertically on Si substrates by non-catalytic vapor-phase epitaxy," Adv. Mater. **14**, 1841-1843 (2002).
20. T. Yatsui, T. Kawazoe, M. Ueda, Y. Yamamoto, M. Kourogi, and M. Ohtsu, "Fabrication of nanometric single zinc and zinc oxide dots by the selective photodissociation of adsorption-phase diethylzinc using a nonresonant optical near field," Appl. Phys. Lett. **81**, 3651-3653 (2002).
21. Y. Kuniya, Y. Deguchi, and M. Ichida, "Physicochemical properties of dimethylzinc, dimethylcadmium and diethylzinc," Appl. Org. Chem. **5**, 337-348 (1991).

1. Introduction

Nanophotonics has been showing great progress, exploiting the unique physical features appearing in light-matter interactions on the nanometer scale [1]. These interactions allow energy transfer and are free from the diffraction of light. High-density optical memories [2], sensors [3], and logic devices [4] have been demonstrated, as well as novel system functions [5] and nano-scale optical characterizations [6].

Fabrication techniques such as those based on lithographic and self-organization approaches are important assets in pursuing such nanophotonic devices and systems. Optical near-field interactions themselves have been successfully applied to fabrication techniques in the literature [7]; since an optical near-field appears locally in the vicinity of a material, it can help in fabricating nano-structures, such as in chemical vapor deposition (CVD) processes where materials are selectively deposited only in the vicinity of a near-field fiber probe tip [8] and in lithography where optical near-fields appears in the surroundings of a mask pattern which induces chemical reactions in a photo-resist [9].

In this paper, with a view to exploiting the unique physical nature of such optical near-fields, we highlight the process of generating smaller-scale structures from larger-scale ones via optical near-field interactions, which is schematically shown in Fig. 1. Usually, the generation of smaller-scale structures involves higher costs in achieving the required fine precision. Instead, if we could produce the intended fine structures with less physically

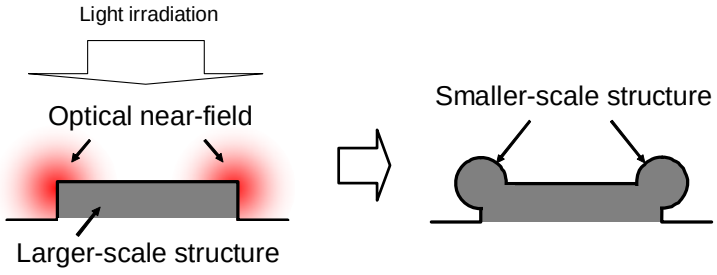

Fig. 1. Generation of smaller-scale structures from larger-scale ones via optical near-field interactions.

#85246 - $15.00 USD Received 13 Jul 2007; revised 29 Aug 2007; accepted 29 Aug 2007; published 31 Aug 2007

demanding resources, manufacturing costs could be reduced. Moreover, since this is a unique ability of optical near-field interactions, it would be technically difficult to mimic the resultant structure using other fabrication methods; therefore, potential applications would include security-related functions, for example, in so-called physical unclonability [10] and so forth.

This paper is organized as follows. In Section 2, we will first describe known physical processes of generating smaller-scale structures from larger-scale ones involving optical near-field interactions. We then present a theoretical framework for such processes using an angular spectrum, which explicitly represents the scale-dependence of optical near-fields. In Section 3, we describe an experimental demonstration of such principles by using ZnO nanoneedles fabricated through metal-organic vapor phase epitaxy (MOVPE) followed by a photo-induced MOVPE procedure, where smaller-scale generated structures were clearly observed with the help of light irradiations. We also observed that the generated fine structures followed a power-law distribution, indicating that fractal structures emerged via optical near-field interactions. Section 4 concludes the paper.

2. Generation of smaller-scale structures via optical near-fields: a theoretical basis

We briefly introduce known physical processes by which smaller-scale structures are generated from larger-scale ones via optical near-field interactions.

[Example 1] Self-assembly of a size- and position-controlled nanodot chain has been successfully demonstrated selectively along the edge of a groove formed in a glass substrate when irradiated with light [11]. A sub-100 nm dot chain was deposited based on the balance between the deposition and desorption, with the dot size depending on the photon energy. Here we find that smaller-scale structures, namely nanodot chains, are generated by globally irradiated light via optical near-fields appearing along the edge of a groove.

[Example 2] When sub-wavelength structures are irradiated with light, either in dielectric or metal, electric polarizations and electric currents are induced within dielectric and metal structures, respectively. For both dielectric and metal structures, we find that surface electric charges are induced at the edges of the structures. Those surface charges then induce strong local electric fields. For instance, in the case of metal nanostructures, such as a bow-tie-shaped metal nanostructure having a small gap between two wedge-shaped metallic plates [12-15], an optical near-field is generated between the two apexes due to the interaction of charges concentrated at those points. Regarding the associated physical scales involved, we can see that strong electric fields are generated in a small area, namely at the gap of the bow-tie, from globally irradiated light over the entire structure.

In order to account for such phenomena theoretically in a general framework, we use an angular spectrum representation of electromagnetic fields [16] to describe optical near-fields [17]. This approach allows analytical treatment and gives an intuitive picture of the localization of optical near-fields in the region a given distance away from the material since it describes electromagnetic fields as a superposition of evanescent waves with different decay lengths and corresponding spatial frequencies. In other words, one can clearly grasp the fact that optical near-fields have a hierarchical nature, meaning that optical near-field at a point of interest originates from a structure whose scale is comparable to the distance between the material and the point of interest [18].

Before modeling smaller-scale generated structures, we first introduce an angular spectrum representation of the radiation from a dipole. Theoretical details can be found in Ref. [17].

Suppose, for example, that we have an oscillating electric dipole, $\boldsymbol{d}^{(k)}$, with frequency K, placed on the *xz* plane, and oriented with respect to the *z* axis by $\theta^{(k)}$. The superscript (*k*) is used to identity dipoles in multiple-dipole systems $(k = 1, \cdots, N)$. The geometrical arrangement of a dipole is explained in the Appendix and in Fig. 5. Here, the speed of light is taken as unity (*c*=1). We consider the electric-field of radiation at a position on the *xz* plane displaced from the dipole $\boldsymbol{d}^{(k)}$ by $\boldsymbol{R} = (r_{\parallel}^{(k)} \cos\varphi^{(k)}, 0, z^{(k)})$. The angular spectrum representation of the *z*-component of the optical near-field is given by

#85246 - $15.00 USD Received 13 Jul 2007; revised 29 Aug 2007; accepted 29 Aug 2007; published 31 Aug 2007

$$E_z(\boldsymbol{r}) = \left(\frac{iK^3}{4\pi\varepsilon_0}\right)\int_1^\infty ds_{\parallel}\,\frac{s_{\parallel}}{s_z}\,f_z(s_{\parallel},\boldsymbol{d}^{(1)},\cdots,\boldsymbol{d}^{(N)}) \tag{1}$$

where

$$f_z(s_{\parallel},\boldsymbol{d}^{(1)},\cdots,\boldsymbol{d}^{(N)}) = \sum_{k=1}^{N}\Big\{d^{(k)}s_{\parallel}\sqrt{s_{\parallel}^2-1}\sin\theta^{(k)}\cos(\phi^{(k)}-\varphi^{(k)})J_1\left(Kr_{\parallel}^{(k)}s_{\parallel}\right)\exp\left(-Kz^{(k)}\sqrt{s_{\parallel}^2-1}\right) \tag{2}$$
$$+d^{(k)}s_{\parallel}^2\cos\theta^{(k)}J_0\left(Kr_{\parallel}^{(k)}s_{\parallel}\right)\exp\left(-Kz^{(k)}\sqrt{s_{\parallel}^2-1}\right)\Big\}.$$

Here, $s_{\parallel}$ is the spatial frequency of an evanescent wave propagating parallel to the *x* axis, and $J_n(x)$ represents Bessel functions of the first kind. We call $f_z(s_{\parallel},\boldsymbol{d}^{(1)},\cdots,\boldsymbol{d}^{(N)})$ the angular spectrum of the electric field [18].

Now, we present a physical model of structures based on multiple dipoles. Suppose that there is a structure whose size is represented by a horizontal length denoted by *L*, as shown by the dashed lines in Fig. 2(a). When we irradiate this structure with light, as described in Section 1 and at the beginning of Section 2, electron charges tend to be concentrated at the corners of the structure. Therefore, as a phenomenological model, we represent such a situation by a two-dipole model, as shown in Fig. 2(a), where the dipoles are labeled $\boldsymbol{d}^{(1)}$ and $\boldsymbol{d}^{(2)}$. We also assume that those dipoles have a phase difference of π and are parallel to the *x* axis; therefore we assume that the orientations of the dipoles are given by $\theta^{(1)} = -\pi/2$ and

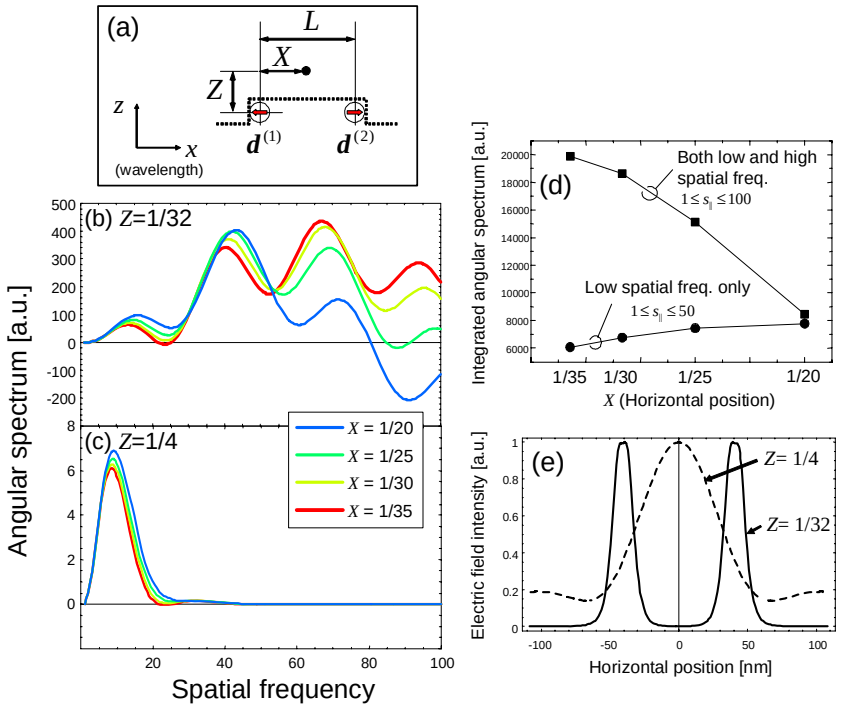

Fig. 2. (a). Physical model based on dipoles ($\boldsymbol{d}^{(1)}$ and $\boldsymbol{d}^{(2)}$) and the points of interest denoted by *X* and *Z*. The size of the larger-scale structure is represented by *L*. Angular spectrum evaluated at positions (b) closer to the structure (*Z* = 1/32), and (c) relatively far from the structure (*Z* = 1/4). The dimensions are represented in units of wavelength. (d) Integrated angular spectrum in the spatial frequency interval of $1 \le s_{\parallel} \le 100$ and $1 \le s_{\parallel} \le 50$ at *Z* = 1/32. (e) Electric field intensity profiles at *Z* = 1/32 (solid curve) and *Z* = 1/4 (dashed curve) calculated through rigorous theoretical modeling.

#85246 - $15.00 USD Received 13 Jul 2007; revised 29 Aug 2007; accepted 29 Aug 2007; published 31 Aug 2007

$\theta^{(2)} = \pi/2$. The distance between the dipoles is given by *L*.

In order to show the scale dependence of optical near-fields in this model, we consider the electric field at a position that is away from the dipole $\boldsymbol{d}^{(1)}$ by distances *X* and *Z* along the *x*-axis and *z*-axis, respectively, as shown in Fig. 2(a). Here, *L*, *X*, and *Z* indicate distances in units of wavelength. If the angular spectrum contains higher spatial frequency components, it means that the electric field is localized at that position to the extent given by that spatial frequency.

Here, we assume that the size of the structure is $L = 1/4$. In order to evaluate localization of optical near-fields in the vicinity of the structure denoted by *L*, first we analyze the region close to the structure, namely *Z* = 1/32. Figure 2(b) represents the angular spectrum at different horizontal distances *X* = 1/20, 1/25, 1/30, and 1/35. We found that at smaller *X*, namely, when *X* is smaller than 1/30, the angular spectrum has positive values in the spatial frequency range denoted by $1 < s_{\|} < 100$. This indicates that electric fields are strongly localized in the region close to $\boldsymbol{d}^{(1)}$, which corresponds to the corner of the large structure denoted by *L*. As the point of interest approaches the midpoint between the dipoles, the angular spectrum has negative values, for example, with the cases *X* = 1/20 and 1/25 in Fig. 2(b), meaning that the localization of the electric field becomes relatively degraded as we get closer to the midpoint between the dipoles, or the midpoint of the large structure denoted by *L*. In other words, a localized electric field appears in the very vicinity of the corner of the structure; a smaller scale structure represented by $\Delta X = 1/30$ appears from a relatively large structure denoted by $L = 1/4$.

Figure 2(e) also demonstrates such a mechanism clearly by integrating the angular spectrum over lower and higher spatial frequencies while *Z* is kept at 1/32. We can see that the integral of the angular spectrum over the domain $1 \le s_{\|} \le 100$, indicated by squares, increases as the horizontal position gets closer to the corner of the structure. On the other hand, the integral of the angular spectrum over the domain $1 \le s_{\|} \le 50$, represented by circles, exhibits nearly the same value regardless of the horizontal position. These results demonstrate that the high spatial-frequency components contribute to the localization of electric fields in the vicinity of the corner of the structure.

In contrast, at a relatively large distance away from the structure, for instance *Z* = 1/4, the angular spectrum exhibits nearly the same distribution regardless of the value of *X*, as shown in Fig. 2(c). This means that the optical near-fields are uniformly distributed at this scale; a smaller-scale structure is not generated at regions far from the large structure denoted by *L*.

In fact, we can derive the electric field distribution at any given point based on a rigorous representation of the electric field, including far-field and near-field components. The solid and dashed curves in Fig. 2(e) respectively show the intensity profiles along the *x* axis at distances far from the dipoles, namely, distances *Z* = 1/32 and 1/4, respectively. Here, we assume a wavelength of 325 nm. We can clearly observe that localization appears strongly in the vicinity of the material (*Z* = 1/32), but does not appear relatively far from the material (*Z* = 1/4).

3. Experiment

To demonstrate such scale-generation processes via optical near-field interactions, we used ZnO nanoneedles as a generator of optical near-fields. The metallic nanostructures were deposited on the ZnO nanoneedles by a photo-induced chemical reaction. The effect of light irradiation was evaluated by comparing the resultant structures grown in the areas where light was irradiated and where it was not.

ZnO nanoneedles were grown on a sapphire (0001) substrate using a metal-organic vapor phase epitaxy (MOVPE) system [19]. Diethyl zinc (Et_2Zn) and oxygen were used as reactants, and they had flow rates ranging from 0.5 to 5 sccm and 20 to 100 sccm, respectively. The deposition temperature was 400 ^{o}C, and the growth time was 1 hour.

#85246 - $15.00 USD Received 13 Jul 2007; revised 29 Aug 2007; accepted 29 Aug 2007; published 31 Aug 2007

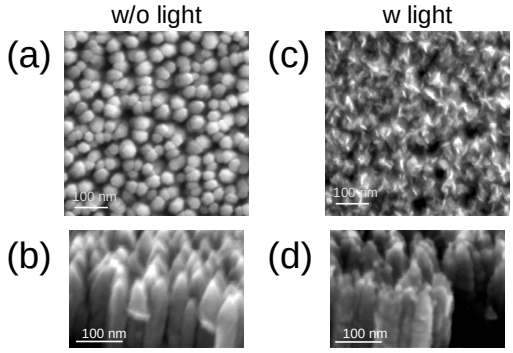

Fig. 3. (a, b) SEM images of ZnO nanoneedle fabricated through metal-organic vapor phase epitaxy (MOVPE). (c, d) SEM images of the same ZnO nanoneedles after photo-induced MOVPE.

The surface morphology of the as-grown ZnO nanoneedles was investigated using scanning electron microscopy (SEM). As shown in Figs. 3(a) and 3(b), a high density of ZnO nanoneedles was vertically aligned over the entire substrate, and they exhibited sharp tips. Typically, the nanoneedles exhibited a mean tip radius of 5 nm, which is expected to generate strong optical near-fields.

After growing the nanoneedles, we deposited Zn nanoparticles on the ZnO nanoneedles. To realize near-field deposition [20], instead of thermal deposition, we conducted deposition using photo-induced chemical reaction at low temperature, so that thermal deposition was negligible. Since the Et_2Zn is dissociated at temperatures exceeding 150 ^oC [21], we deposited Zn at 60 ^oC and used a He-Cd laser with a wavelength of 325 nm as a light source for dissociating the Et_2Zn. The flow rates of Et_2Zn including Ar carrier gas ranged from 20 to 100 sccm. We irradiated He-Cd laser light with an average power of 1 mW for 5 minutes.

Figures 3(a) and 3(b) show SEM pictures of nanoneedles fabricated in the areas without light illumination (w/o light), and Figs. 3(c) and 3(d) show those fabricated with light illumination (w light). As is clear from the cases with light irradiation [Figs. 3(c) and 3(d)], fine structures appeared at the apex and vertex of the nanoneedles. We attributed the generation of these fine structures to the optical near-field interactions induced by the nanoneedles, which accelerated the deposition rate of Zn nanoparticles.

We then numerically demonstrated the effect of smaller-scale generation. We analyzed the SEM images to determine the representative scales; these are highlighted as shown in Figs. 4(a) and 4(b), which were digitized from Figs. 3(a) and 3(c), respectively. Physically, Fig. 4(a) represents the projected area of the ZnO nanoneedles, and Fig. 4(b) shows that of deposited Zn on top of the ZnO nanoneedles. We evaluated the representative scales, denoted by *S*, by the horizontal extent of the structures, as schematically shown in Fig. 4(c). The incidence of these scales *S* was measured from all rows in the images. Figures 4(a) and 4(b) are respectively composed of 510×510 pixels and 591×591 pixels, but occupy the same area of $576\ \text{nm} \times 576\ \text{nm}$.

Figure 4(d) shows the incidence of the scales *S*, where the square and circular marks indicate the structures fabricated, without light and with light, respectively. The structures fabricated without light exhibited a maximum incidence around 30 nm, which refers to the representative scale *S* of this structure. On the other hand, the structures fabricated with light exhibited a quite different incidence pattern with smaller scales and higher populations. In other words, smaller-scale structures were generated from larger-scale ones though the light irradiation process, which induced optical near-field interactions.

#85246 - $15.00 USD Received 13 Jul 2007; revised 29 Aug 2007; accepted 29 Aug 2007; published 31 Aug 2007

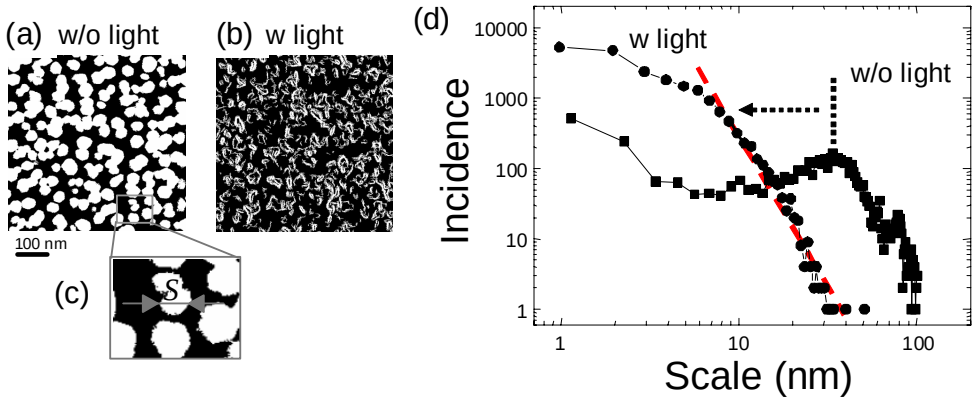

Fig. 4. Analysis of scales in the structures fabricated without light and with light. (a) Images of the structures fabricated (a) without light and (b) with light, which are obtained from Fig. 3(a) and (c), respectively. (c) The horizontal extent of the structure used for analysis of the scales denoted by *S*. (d) Incidence of the scales in (a) and (b).

Furthermore, it should also be noted that the histogram of the structures fabricated with light exhibits a power-law distribution; the square marks were fitted to a straight line in a double logarithmic plot at scales larger than around 6 nm. The incidence of the scale *S* follows $y = 5\times10^{6} S^{-4.24}$, denoted by a red dashed line in Fig. 4(d), where *y* represents the incidence. This means that a fractal nature emerged from a non-fractal structure in the scale merit defined above. We are now studying the origin of this fractal behavior based on analysis of the geometries of the ZnO nanoneedles and the dynamics involved in optical near-fields appearing in the vicinity of nanoneedles, as well as their associated Zn deposition processes.

4. Conclusion

We have demonstrated the generation of smaller-scale structures from larger-scale structures via optical near-field interactions. A theoretical framework is shown based on an angular spectrum representation of optical near-fields, which allows intuitive insights regarding their scale dependence. Experimental demonstrations are also shown using ZnO nanoneedles fabricated through standard MOVPE and Zn nanoparticles deposited through photo-induced MOVPE processes. The incidence of the representative scale clearly shifted to smaller values in the presence of light irradiation. The emergence of fractal behavior was also observed. We are now pursuing further analysis of such small-scale generation processes both theoretically and experimentally. We are also seeking potential applications of these unique physical processes involving optical near-field interactions, such as security applications.

Acknowledgments

The authors are indebted to Prof. Gyu-Chul Yi of Pohang University of Science and Technology (POSTECH), Pohang, Korea for their support in fabricating the nanoneedles.

#85246 - $15.00 USD Received 13 Jul 2007; revised 29 Aug 2007; accepted 29 Aug 2007; published 31 Aug 2007

Appendix

The geometrical arrangement of a dipole, denoted by $\boldsymbol{d}^{(k)}$, which is placed at the origin of a three dimensional Cartesian space is shown in Fig. 5. The angular spectrum representation of the electric field given by Eqs. (1) and (2) are based on this arrangement. The dipole $\boldsymbol{d}^{(k)}$ is placed on the *xz* plane and oriented with respect to the *z* axis by $\theta^{(k)}$. The point of interest, denoted by *P*, is displaced from the dipole by $\boldsymbol{R} = (r_{\parallel}^{(k)} \cos\varphi^{(k)}, r_{\parallel}^{(k)} \sin\varphi^{(k)}, z^{(k)})$. Since our analysis shown in Section 2 focuses on two-dimensional space, namely, on the *xz* plane, the angle takes the value 0 or π; $\varphi^{(k)} = 0$ if the point of interest is located at the positive side of the dipole along the *x* axis, and $\varphi^{(k)} = \pi$ if it is placed on the negative side of the dipole along the *x* axis.

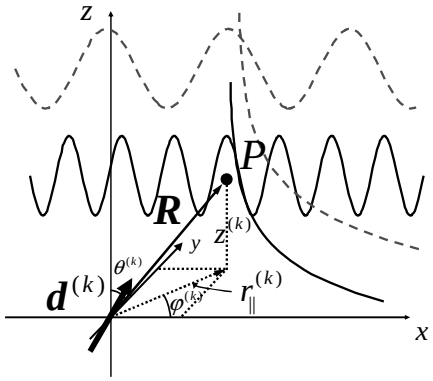

Fig. 5. Geometrical arrangement of a dipole and a point of interest.

#85246 - $15.00 USD Received 13 Jul 2007; revised 29 Aug 2007; accepted 29 Aug 2007; published 31 Aug 2007